

# Statistics of the Nonlinear Discrete Spectrum of a Noisy Pulse

Francisco Javier García-Gómez and Vahid Aref

**Abstract**—In the presence of additive Gaussian noise, the statistics of the nonlinear Fourier transform (NFT) of a pulse are not yet completely known in closed form. In this paper, we propose a novel approach to study this problem. Our contributions are twofold: first, we extend the existing Fourier Collocation (FC) method to compute the whole discrete spectrum (eigenvalues and spectral amplitudes). We show numerically that the accuracy of FC is comparable to the state-of-the-art NFT algorithms. Second, we apply perturbation theory of linear operators to derive analytic expressions for the joint statistics of the eigenvalues and the spectral amplitudes when a pulse is contaminated by additive Gaussian noise. Our analytic expressions closely match the empirical statistics obtained through simulations.

**Index Terms**—Nonlinear Fourier Transform, Nonlinear Frequency Division Multiplexing, Multi-soliton, Fourier collocation

## I. INTRODUCTION

The Nonlinear Fourier Transform (NFT), or Inverse Scattering Transform [1], [2] has been proposed as an alternative for system design in an attempt to overcome the capacity peak reported in [3] of linear transmission systems over the nonlinear optical channel. An overview on the NFT and its application for optical communications is given in [4].

Communication using the NFT (continuous or discrete spectrum) has been demonstrated numerically and experimentally, e.g. [4]–[9]. Despite some promising results, the effect of channel noise on the NFT is not yet well understood. Recently, a general method has been developed in [10] to numerically compute the statistics of the spectral coefficients (not the eigenvalues) of a signal with additive white Gaussian noise (AWGN). This method, however, requires knowledge of the time-domain signal. In the case of propagation along an optical fiber with *distributed* AWGN along the fiber, the statistics of the NFT of a first-order soliton are well known [11]–[13]. Recently, the statistics of the eigenvalues of an arbitrary pulse with the same propagation model were derived [14]. All these results were obtained based on some perturbative methods.

This work builds up on our previous paper [15] and makes a twofold contribution. First, we extend the existing Fourier Collocation (FC) method [16, Sec. 2.4.3] to compute the complete discrete spectrum (eigenvalues and spectral amplitudes) of arbitrary pulses. We apply a proper windowing and truncation to overcome the ringing problem caused by non-periodic boundary conditions of NFT. Our simulations show

that our method achieves a comparable accuracy to the best existing methods when the number of time samples is low.

Second, we apply the perturbation theory of matrix eigenvalues [17] to our extended method to derive the statistics of the discrete spectrum when a pulse is contaminated by Gaussian noise. Note that the eigenvalue perturbation theory is also used in [2, Part III, Sec. IV-A] and [14] to find the statistics of the eigenvalues. Our method is novel in two aspects: we analyze the statistics in the frequency domain, and we provide a single method to compute both eigenvalues and spectral amplitudes, thus allowing computation of cross-correlations between the two. We show that our analytic expressions for the statistics of the discrete spectrum closely match the statistics obtained through Monte-Carlo simulations.

The paper is organized as follows. In Sec. II, we briefly overview the NFT and the multi-soliton pulses. In Sec. III, we describe the FC method and extend it to compute also the discrete spectral amplitudes by proper windowing and truncation. Applying a first-order perturbation method, we derive the statistics of the discrete spectrum for an arbitrary pulse in Sec. IV. We validate in Sec. V both our extended FC method and our analytic expressions for the statistics of the discrete spectrum through simulations with different pulses. Sec. VI concludes the paper.

*Notation:* Bold lowercase letters  $\mathbf{x}$  denote vectors, and bold uppercase letters  $\mathbf{X}$  denote matrices.  $\mathbf{X}^T$  and  $\mathbf{X}^H$  are respectively the transpose and conjugate transpose of  $\mathbf{X}$ .  $(\mathbf{x}, \mathbf{y})$  is the horizontal concatenation of vectors  $\mathbf{x}$  and  $\mathbf{y}$ .  $\Re x$  is the real part of  $x$ , and  $\Im x$  is its imaginary part.

## II. SYSTEM MODEL

Consider the complex envelope  $A(Z, \tau)$  of an electrical field propagating along an optical fiber, where  $Z$  is distance and  $\tau$  is time. The propagation is modeled by the Nonlinear Schrödinger Equation (NLSE) [18, Eq. (2.3.46)]:

$$\frac{\partial A(Z, \tau)}{\partial Z} = -j \frac{\beta_2}{2} \frac{\partial^2 A(Z, \tau)}{\partial T^2} + j\gamma |A(Z, \tau)|^2 A(Z, \tau) \quad (1)$$

where  $\beta_2$  is the chromatic dispersion parameter, and  $\gamma$  is the nonlinear coefficient. We neglect attenuation in (1) assuming that it is compensated by distributed amplification. With proper normalization [2], the NLSE can be transformed to

$$\frac{\partial}{\partial z} q(z, t) = j \frac{\partial^2}{\partial t^2} q(z, t) + j2 |q(z, t)|^2 q(z, t) \quad (2)$$

where  $q$  is the normalized signal,  $t$  is the normalized time, and  $z$  is the normalized distance.

Date of current version April 19, 2019. J. García-Gómez is with the Institute for Communications Engineering (LNT), Technical University of Munich, Germany (e-mail: javier.garcia@tum.de). His work was supported by the German Research Foundation under Grant KR 3517/8-1.

V. Aref is with Nokia Bell Labs, Stuttgart 70435, Germany (e-mail: vahid.aref@nokia-bell-labs.com).

### A. Description in Nonlinear Spectrum

The NFT is calculated by solving the Zakharov-Shabat system (ZSS) [1], [2]

$$\begin{pmatrix} -\frac{\partial}{\partial t} & q(t) \\ q^*(t) & \frac{\partial}{\partial t} \end{pmatrix} \begin{pmatrix} v_1(t, \lambda) \\ v_2(t, \lambda) \end{pmatrix} = j\lambda \begin{pmatrix} v_1(t, \lambda) \\ v_2(t, \lambda) \end{pmatrix} \quad (3)$$

with the boundary condition

$$\mathbf{v}(t, \lambda) \rightarrow \begin{pmatrix} 1 \\ 0 \end{pmatrix} e^{-j\lambda t}, \quad t \rightarrow -\infty \quad (4)$$

where  $\mathbf{v}(t, \lambda) = (v_1(t, \lambda)v_2(t, \lambda))^T$  is the *Jost solution*. The *spectral coefficients*  $a(\lambda)$  and  $b(\lambda)$  are given by

$$a(\lambda) = \lim_{t \rightarrow \infty} v_1(t, \lambda) e^{j\lambda t} \quad (5a)$$

$$b(\lambda) = \lim_{t \rightarrow \infty} v_2(t, \lambda) e^{-j\lambda t}. \quad (5b)$$

The NFT of the signal  $q(t)$  is made up of two spectra:

- the *continuous spectrum*  $Q(\xi) = \frac{b(\xi)}{a(\xi)}$ , for  $\xi \in \mathbb{R}$ ;
- the *discrete spectrum*  $Q_k = \frac{b(\lambda_k)}{a_\lambda(\lambda_k)}$ , for the  $K$  eigenvalues  $\{\lambda_k \in \mathbb{C}^+ : a(\lambda_k) = 0\}$

where  $a_\lambda = da/d\lambda$  and  $\mathbb{C}^+ = \{\lambda \in \mathbb{C} : \Im \lambda > 0\}$ .

In recent works [8], [9], [19], the use of  $b_k = b(\lambda_k)$  instead of  $Q_k$  for data modulation in the discrete spectrum has been shown to achieve better results. In terms of degrees of freedom, both approaches are equivalent, as given  $\lambda_k$  and  $b(\xi)$  for  $\xi \in \mathbb{R}$ , one can compute  $a(\lambda)$  as [20, Ch. I, Eq. (6.23)]

$$a(\lambda) = \exp \left[ \frac{1}{2\pi j} \int_{-\infty}^{\infty} \frac{\log(1 - |b(\xi)|^2)}{\xi - \lambda} d\xi \right] \prod_{k=1}^K \frac{\lambda - \lambda_k}{\lambda - \lambda_k^*}. \quad (6)$$

For this reason, in this paper we obtain the statistics of  $\lambda_k$  and  $b_k$ , but not of  $Q_k$ . The usefulness of the NFT lies in the fact that, given a signal  $q(z, t)$  propagating according to the NLSE (2), the evolution of its NFT in  $z$  is multiplicative:

$$\begin{aligned} Q(z, \xi) &= Q(0, \xi) e^{4j\xi^2 z} & \lambda_k(z) &= \lambda_k(0) \\ b_k(z) &= b_k(0) e^{4j\lambda_k^2 z} & a(z, \lambda) &= a(0, \lambda). \end{aligned} \quad (7)$$

We skip index  $z$  in the sequel for simplicity. Many numerical algorithms have been developed to compute NFT (e.g., [2], [4]). As a benchmark, we use in this paper the forward-backward iterations [21], [22] combined with a recently proposed algorithm in [23] with a sixth-order Commutator-Free Quasi-Magnus (CFQM) integrator  $\text{CF}_4^{[6]}$ . Its sixth-order accuracy is the best we have found in the literature. We replace the trapezoidal integration of [22] with the CFQM to improve the performance. We call this algorithm FB-CFQM.

### B. Multi-soliton Pulses

A *multi-soliton pulse* has no continuous spectrum, i.e.,  $b(\xi) = 0$ . In Algorithm 1, we provide pseudo-code that uses the Darboux transform [24] to construct a time-domain multi-soliton pulse and its Jost solutions from the discrete spectrum. Some other Inverse NFT algorithms are reviewed in [4].

---

**Algorithm 1:** Darboux Transform to compute  $K$ -soliton  $q(t)$  and its Jost Solutions  $\mathbf{v}_k(t) \triangleq \mathbf{v}(t, \lambda_k)$ ,  $1 \leq k \leq K$  from discrete spectrum  $\{(\lambda_k, b_k)\}_{k=1}^K$ .

---

```

/* initialize the Jost solutions  $\mathbf{v}_k^{(0)}(t)$ .
The superscript  $(i)$  indicates the
algorithm iteration number */
for  $k \leftarrow 1$  to  $K$  do
     $\mathbf{v}_k^{(0)}(t) = (e^{-j\lambda_k t}, -b_k e^{j\lambda_k t})^T$ ;
end
 $q^{(0)}(t) = 0$ ;
/* iteratively add  $(\lambda_i, b_i)$  */
for  $i \leftarrow 1$  to  $K$  do
     $(f_1, f_2) = \mathbf{v}_i^{(i-1)}(t)$ ;
    /* update signal */
     $q^{(i)}(t) = q^{(i-1)}(t) - 2j(\lambda_i - \lambda_i^*) \frac{f_2^*(t)f_1(t)}{|f_1(t)|^2 + |f_2(t)|^2}$ ;
    /* update  $\mathbf{v}_i^{(i)}(t)$  */
     $C = b_i \prod_{k=1}^{i-1} (\lambda_i - \lambda_k) \prod_{k=i+1}^K 1/(\lambda_i - \lambda_k^*)$ ;
     $\mathbf{v}_i^{(i)}(t) = \frac{C}{|f_1(t)|^2 + |f_2(t)|^2} \begin{pmatrix} -f_2^*(t) \\ f_1^*(t) \end{pmatrix}$ ;
    /* update  $\mathbf{v}_k^{(i)}(t) \triangleq (v_{k,1}^{(i)}(t), v_{k,2}^{(i)}(t))^T$  */
    for  $k \leftarrow 1$  to  $K$ ;  $k \neq i$  do
         $v_{k,1}^{(i)}(t) = \left( \lambda_k - \lambda_i^* - \frac{(\lambda_i - \lambda_i^*)|f_1(t)|^2}{|f_1(t)|^2 + |f_2(t)|^2} \right) v_{k,1}^{(i-1)}(t) -$ 
 $\frac{(\lambda_i - \lambda_i^*)f_2^*(t)f_1(t)}{|f_1(t)|^2 + |f_2(t)|^2} v_{k,2}^{(i-1)}(t)$ ;
         $v_{k,2}^{(i)}(t) = -\frac{(\lambda_i - \lambda_i^*)f_2(t)f_1^*(t)}{|f_1(t)|^2 + |f_2(t)|^2} v_{k,1}^{(i-1)}(t) +$ 
 $\left( \lambda_k - \lambda_i + \frac{(\lambda_i - \lambda_i^*)|f_1(t)|^2}{|f_1(t)|^2 + |f_2(t)|^2} \right) v_{k,2}^{(i-1)}(t)$ ;
    end
end
Output:  $q(t) = q^{(K)}(t)$  and  $\mathbf{v}(t, \lambda_i) = \mathbf{v}_i^{(K)}(t)$ 

```

---

### III. THE FOURIER COLLOCATION (FC) METHOD

The FC method [16, Sec. 2.4.3], or *spectral method* [2, Part II] finds the discrete eigenvalues of the NFT of a signal  $q(t)$ . This is done by setting up a matrix eigenvalue problem in the linear frequency domain. Assume that  $q(t)$  is only nonzero in a finite time interval<sup>1</sup>  $[-T/2, T/2]$ . In this case, we can trivially compute  $\mathbf{v}(t, \lambda)$  for  $t \notin [-T/2, T/2]$  in terms of  $\mathbf{v}(\pm T/2, \lambda)$ . We need only to find  $\mathbf{v}(t, \lambda)$  for  $t \in [-T/2, T/2]$ .

Assume that the periodic extensions with period  $T$  of  $q(t)$  and  $v_i(t, \lambda_k)$  for  $t \in [-T/2, T/2]$  are band-limited to the frequency band  $[-N/T, N/T]$ , where  $N$  is an integer. By performing these periodic extensions, we can express  $q(t)$  and  $v_i(t, \lambda_k)$  for  $t \in [-T/2, T/2]$  and  $i \in \{1, 2\}$  by a Fourier series of  $M = 2N + 1$  terms

$$q(t) = \sum_{n=-N}^N c[n] e^{jn\frac{2\pi}{T}t}, \quad v_i(t, \lambda_k) = \sum_{n=-N}^N \psi_{k,i}[n] e^{jn\frac{2\pi}{T}t}. \quad (8)$$

The Fourier coefficients can be then computed as a discrete Fourier transform (DFT) of the sampled pulses. Define  $q[m] =$

<sup>1</sup>A pulse  $q(t)$  can be confined in  $[-T/2, T/2]$  by a time-shift  $t_0$ . The spectrum of  $q(t-t_0)$  has the same  $\lambda_k$  but the  $b$ -coefficients are  $b_k \exp(-j\lambda_k t_0)$ .

$q(t_m)$  where  $t_m = m\frac{T}{M}, m \in \{-N, \dots, N\}$ . Hence,

$$c[n] = \frac{1}{M} \sum_{m=-N}^N q[m] e^{-j\frac{2\pi}{M}mn}. \quad (9)$$

In a similar manner,  $\psi_{k,i}[n]$  can be obtained from  $v_{k,i}[m] = v_i(t_m, \lambda_k)$  for  $i \in \{1, 2\}$ . Let  $\Psi_k = (\psi_{k,1}[-N], \dots, \psi_{k,1}[N], \psi_{k,2}[-N], \dots, \psi_{k,2}[N])^T$ . Substituting (8) into (3) yields

$$\mathbf{L}\Psi_k = \lambda_k\Psi_k \quad (10)$$

where

$$\mathbf{L} = \begin{pmatrix} \mathbf{\Omega} & \mathbf{\Gamma} \\ -\mathbf{\Gamma}^H & -\mathbf{\Omega} \end{pmatrix}, \quad (11)$$

$\mathbf{\Omega} = -\frac{2\pi}{T}\text{diag}(-N, \dots, N)$ , and  $\mathbf{\Gamma} \in \mathbb{C}^{M \times M}$  is a Toeplitz matrix whose first column is  $-j(c[0], \dots, c[N], 0, \dots, 0)^T$  and whose first row is  $-j(c[0], \dots, c[-N], \dots, 0)$ .

A solution  $(\lambda_k, \Psi_k)$  of (10) corresponds to the Fourier coefficients of a solution  $\mathbf{v}(t, \lambda_k)$  of the ZSS (3). Accordingly, the eigenvalues of  $\mathbf{L}$  include the eigenvalues  $\lambda_k$  of the discrete spectrum, their complex conjugates, and  $M - 2K$  spurious eigenvalues which are usually observed with rather small imaginary parts.

#### Computation of Spectral Amplitudes $b_k$

We extend the FC method to also compute the spectral amplitudes  $b_k$ . The IDFT of any  $\lambda_k$ -eigenvector  $\Psi_k$  of (10) is an eigenvector of (3). As any multiple of an eigenvector is also an eigenvector, we have

$$\sum_{n=-N}^N \psi_{k,i}[n] e^{jn\frac{2\pi}{T}t} = G_k v_i(t, \lambda_k) \quad (12)$$

for some constant  $G_k$ . Setting  $v_1(-T/2, \lambda_k) = \exp(-j\lambda_k(-T/2))$  in (12) to satisfy (4), we obtain

$$G_k = e^{j\lambda_k(-\frac{T}{2})} \sum_{n=-N}^N \psi_{k,1}[n] e^{jn\frac{2\pi}{T}(-\frac{T}{2})}. \quad (13)$$

Note that (4) imposes two boundary conditions. We observed in our simulations that the other condition  $v_2(-T/2, \lambda_k) \approx 0$  in (12) was always numerically satisfied, as expected. From (5), we have  $b_k = v_2(T/2, \lambda_k) \exp(-j\lambda_k T/2)$ . Substituting this in (12), we have

$$b_k = \frac{e^{-j\lambda_k \frac{T}{2}}}{G_k} \sum_{n=-N}^N \psi_{k,2}[n] e^{jn\frac{2\pi}{T} \frac{T}{2}}. \quad (14)$$

The above quantities are based on the assumption that the periodic extensions of  $v_i(t, \lambda_k)$  for  $i \in \{1, 2\}$  have a bandwidth smaller than  $2N/T$ . However, this assumption may not be satisfied if  $v_i(-T/2, \lambda_k) \neq v_i(T/2, \lambda_k)$  (note that, for  $T \rightarrow \infty$  we have  $v_i(-T/2, \lambda_k) = v_i(T/2, \lambda_k) \rightarrow 0$ , but this holds only approximately for finite  $T$ ). This may cause undesirable ripples on  $v_i(t, \lambda_k)$  around  $t = \pm T/2$  when  $v_i(t, \lambda_k)$  is obtained from (8). The ripples have a severe impact on the estimation of  $G_k = v_1(-T/2, \lambda_k) e^{-j\lambda_k T/2}$  and

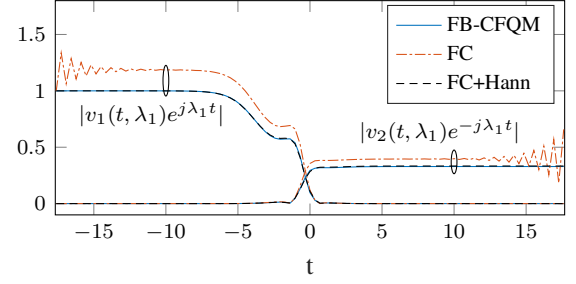


Fig. 1. Computation of  $|v_1(t, \lambda_1)e^{j\lambda_1 t}|$  and  $|v_2(t, \lambda_1)e^{-j\lambda_1 t}|$  for a 2-soliton ( $T = 35.34$ ). Note the ringing artifact of FC at the edges where  $G_k$  (13) and  $b_k$  (14) are calculated.

$b_k = v_2(T/2, \lambda_k) e^{-j\lambda_k T/2} / G_k$ . For example, consider a 2-soliton with  $\lambda_1 = 0.6j, \lambda_2 = 0.3j$  and  $b_1 = b_2 = \frac{1}{3}j$ . The signal is truncated to  $t \in [-17.67, 17.67]$  and sampled with  $M = 103$ . We computed  $v_1(t, \lambda_1)e^{j\lambda_1 t}$  and  $v_2(t, \lambda_1)e^{-j\lambda_1 t}$  using FB-CFQM and FC. The results in Fig. 1 show that the FC generates large ripples causing further an incorrect estimate of  $G_k$ . We apply two techniques to mitigate the effect of ripples:

- *Frequency-domain windowing*: we apply windowing functions  $w_1[n]$  and  $w_2[n]$  respectively to  $\Psi_{k,1}$  and  $\Psi_{k,2}$ , the two halves of  $\Psi_k$ . In our simulations, a Hann windowing function [25] gave promising results, as shown by the curves labeled “FC+Hann” in Fig. 1.
- *Tail truncation*: we neglect part of the tails of  $v_1(t, \lambda_k)$  and  $v_2(t, \lambda_k)$  before computing  $G_k$  and  $b_k$ . This means that we replace  $T/2$  with  $T_k < T/2$  in (13), and (14).

In Fig. 1, frequency-domain windowing seems to completely remove the ringing. For more complicated pulses, such as a 5-soliton, tail truncation becomes also necessary. Define the frequency-shifted windows  $u_{k,1}[n]$  and  $u_{k,2}[n]$  as

$$u_{k,1}[n] = w_1[n] e^{-jn\frac{2\pi}{T}T_k} \quad (15)$$

$$u_{k,2}[n] = w_2[n] e^{jn\frac{2\pi}{T}T_k}. \quad (16)$$

Let  $\mathbf{u}_{k,i} = (u_{k,i}[-N], \dots, u_{k,i}[N])^T$ , with  $i \in \{1, 2\}$ . Then, from (13) and (14),  $b_k$  becomes

$$b_k = \frac{\sum_{n=-N}^N w_2[n] \psi_{k,2}[n] e^{jn\frac{2\pi}{T}T_k}}{\sum_{n=-N}^N w_1[n] \psi_{k,1}[n] e^{-jn\frac{2\pi}{T}T_k}} = \frac{\mathbf{u}_{k,2}^T \Psi_{k,2}}{\mathbf{u}_{k,1}^T \Psi_{k,1}}. \quad (17)$$

The choice of  $T_k$  should avoid the ripples in Fig. 1 while staying close enough to the limit value. We choose  $T_k = \min(t_{\text{exp}}, t_{5\%})$ , with:

- $t_{\text{exp}} = 12/\Im\lambda_k$  (such that  $e^{\pm j\lambda_k t}$  does not become larger than  $e^{12} \approx 1.63 \cdot 10^5$ ).
- $t_{5\%} = T/2 - 0.05T$  (5% removed tail).

In our simulations, this heuristic choice works for signals that have most of their energy inside the interval  $[-t_{\text{exp}}, t_{\text{exp}}]$ , which seems to be the case for, at least, solitons of order up to 5 with  $e^{-\Im\lambda_k} < |b_k| < e^{\Im\lambda_k}$ . This heuristic is based on the condition  $|b_k| = 1$  for symmetric solitons, which have good energy confinement in time [26]. For signals known to have high energy outside  $[-t_{\text{exp}}, t_{\text{exp}}]$ , the value of  $t_{\text{exp}}$  can be increased at the cost of accuracy in  $b_k$ . Note

that windowing and truncation are done after obtaining  $\lambda_k$  from (10). Therefore, these two techniques affect only the computation of  $b_k$ .

#### IV. STATISTICS OF THE DISCRETE SPECTRUM

In this section, we derive the second-order statistics of the discrete spectrum of a pulse contaminated by additive Gaussian noise. For this purpose, we apply the well-established perturbation theory of linear operators to the FC method.

Consider again the signal  $q(t)$  of pulse duration  $T$  contaminated by zero-mean additive Gaussian noise  $\sigma\tilde{q}(t)$  that is wide-sense stationary (WSS), i.e.,  $\mathbb{E}[\tilde{q}(t)\tilde{q}^*(t+\tau)] = r_q(\tau)$  does not depend on  $t$ . Here,  $\sigma^2$  is chosen such that  $\mathbb{E}[|\tilde{q}(t)|^2] = 1$ . Let us first assume that  $\sigma\tilde{q}(t)$  has bandwidth  $\mathcal{B}$  and a constant power spectral density (PSD)  $N_0$  inside the band. This implies  $\sigma^2 = N_0\mathcal{B}$ . If the signal is sampled at the Nyquist rate, i.e.,  $\mathcal{B} = M/T$ , then we have for  $m \in \{-N, \dots, N\}$

$$\hat{q}[m] = q[m] + \sigma\tilde{q}[m] \quad (18)$$

where  $\sigma\tilde{q}[m]$  are the zero-mean noise samples. The DFT coefficients of the noisy pulse are

$$\begin{aligned} \hat{c}[n] &= \frac{1}{M} \sum_{m=-N}^N q[m]e^{-j\frac{2\pi}{M}mn} + \frac{\sigma}{M} \sum_{m=-N}^N \tilde{q}[m]e^{-j\frac{2\pi}{M}mn} \\ &= c[n] + \sigma\tilde{c}[n] \end{aligned} \quad (19)$$

where the choice of  $\sigma$  implies that  $\mathbb{E}[\sum_n |\tilde{c}[n]|^2] = 1$ . Define  $\tilde{\mathbf{c}} = (\tilde{c}[-N], \dots, \tilde{c}[N])^T$ . The covariance matrix of the vector  $(\Re\tilde{\mathbf{c}}^T, \Im\tilde{\mathbf{c}}^T)^T$  is

$$\mathbf{R}_{\tilde{\mathbf{c}}} \triangleq \begin{bmatrix} \mathbb{E}[\Re\tilde{\mathbf{c}}\Re\tilde{\mathbf{c}}^T] & \mathbb{E}[\Re\tilde{\mathbf{c}}\Im\tilde{\mathbf{c}}^T] \\ \mathbb{E}[\Im\tilde{\mathbf{c}}\Re\tilde{\mathbf{c}}^T] & \mathbb{E}[\Im\tilde{\mathbf{c}}\Im\tilde{\mathbf{c}}^T] \end{bmatrix} = \frac{1}{2M}\mathbf{1} \quad (20)$$

where  $\mathbf{1}$  is the identity matrix. This is the case of additive white Gaussian noise (AWGN). In a general case with colored noise,  $(\Re\tilde{\mathbf{c}}^T, \Im\tilde{\mathbf{c}}^T)^T = \mathbf{G}\mathbf{w}$ , where  $\mathbf{w}$  is a vector of  $2M$  real-valued, i.i.d. Gaussian variables with variance  $1/(2M)$  and  $\mathbf{G} \in \mathbb{R}^{2M \times 2M}$  satisfies  $\text{tr}(\mathbf{G}\mathbf{G}^T) = 2M$ . Then we have

$$\mathbf{R}_{\tilde{\mathbf{c}}} = \frac{1}{2M}\mathbf{G}\mathbf{G}^T. \quad (21)$$

##### A. Perturbation of the Discrete Spectrum

Let  $\{(\hat{\lambda}_k, \hat{b}_k)\}$  denote the discrete spectrum of the noisy signal. Using the FC method, they are obtained from the solutions of the eigenvalue problem,

$$\hat{\mathbf{L}}\hat{\boldsymbol{\psi}}_k = \hat{\lambda}_k\hat{\boldsymbol{\psi}}_k \quad (22)$$

where

$$\hat{\mathbf{L}} = \mathbf{L} + \sigma\tilde{\mathbf{L}}, \quad (23)$$

where  $\mathbf{L}$ , given in (11), corresponds to the noiseless pulse and

$$\tilde{\mathbf{L}} = \begin{pmatrix} \mathbf{0} & \tilde{\boldsymbol{\Gamma}} \\ -\tilde{\boldsymbol{\Gamma}}^H & \mathbf{0} \end{pmatrix} \quad (24)$$

where  $\tilde{\boldsymbol{\Gamma}} \in \mathbb{C}^{M \times M}$  is a Toeplitz matrix whose first column is  $-j(\tilde{c}[0] \dots \tilde{c}[N] \ 0 \dots 0)^T$  and whose first row is

$-j(\tilde{c}[0] \dots \tilde{c}[-N] \ 0 \dots 0)$ . When  $\sigma^2$  is relatively small,  $(\hat{\lambda}_k, \hat{b}_k)$  can be approximated by first-order perturbations

$$\hat{\lambda}_k = \lambda_k + \sigma\tilde{\lambda}_k + \mathcal{O}(\sigma^2) \quad (25)$$

$$\hat{\boldsymbol{\psi}}_k = \boldsymbol{\psi}_k + \sigma\tilde{\boldsymbol{\psi}}_k + \mathcal{O}(\sigma^2) \quad (26)$$

$$\hat{b}_k = b_k + \sigma\tilde{b}_k + \mathcal{O}(\sigma^2). \quad (27)$$

The perturbation analysis of eigenvalues and eigenvectors is a mature topic. A detailed analysis is given in [17, Sections II.1 and II.2]. We enclose some relevant first-order results as Theorem 1. We first define the left eigenvector  $\boldsymbol{\Phi}_k$  as

$$\boldsymbol{\Phi}_k^H \mathbf{L} = \lambda_k \boldsymbol{\Phi}_k^H. \quad (28)$$

For our operator  $\mathbf{L}$ ,  $\boldsymbol{\Phi}_k$  is equal to the flipped, conjugated version of the right eigenvector  $\boldsymbol{\psi}_k$ , i.e.

$$\boldsymbol{\Phi}_k = (\psi_{k,2}^*[N], \dots, \psi_{k,2}^*[-N], \psi_{k,1}^*[N], \dots, \psi_{k,1}^*[-N])^T. \quad (29)$$

The reason is that  $\boldsymbol{\Phi}_k$  corresponds to the (right) eigenvector of  $\lambda_k^*$  for the signal  $-q(t)$ . This can be seen by taking the conjugate transpose from both sides of (28). Moreover, if  $(\lambda_k, (v_{k,1} \ v_{k,2})^T)$  is a solution of (3) for  $q(t)$ , then  $(\lambda_k^*, (v_{k,2}^* \ v_{k,1}^*)^T)$  is a solution of (3) for  $-q(t)$ . Combining these two properties concludes (29).

**Theorem 1.** Consider (23) with the condition that  $\|\sigma\tilde{\mathbf{L}}\|_F \ll \|\mathbf{L}\|_F$  ( $\|\cdot\|_F$  is the Frobenius norm). We define for every eigenvalue and eigenvectors  $(\lambda_k, \boldsymbol{\psi}_k, \boldsymbol{\Phi}_k)$  of  $\mathbf{L}$

$$\mathbf{P}_k = \frac{1}{\boldsymbol{\Phi}_k^H \boldsymbol{\psi}_k} \boldsymbol{\psi}_k \boldsymbol{\Phi}_k^H \quad (30)$$

$$\mathbf{S}_k = (\mathbf{L} - \lambda_k \mathbf{1} - \mathbf{P}_k)^{-1} (\mathbf{1} - \mathbf{P}_k). \quad (31)$$

The matrix  $\mathbf{P}_k$  is called the eigenprojector of  $\lambda_k$  and  $\mathbf{S}_k$  is the Drazin inverse [27] of  $\mathbf{L} - \lambda_k \mathbf{1}$ . If  $\lambda_k$  has algebraic multiplicity 1, then its first-order perturbations (25) and (26) are given by,

$$\tilde{\lambda}_k = \frac{1}{\boldsymbol{\Phi}_k^H \boldsymbol{\psi}_k} \boldsymbol{\Phi}_k^H \tilde{\mathbf{L}} \boldsymbol{\psi}_k \quad (32)$$

$$\tilde{\boldsymbol{\psi}}_k = -\mathbf{S}_k \tilde{\mathbf{L}} \boldsymbol{\psi}_k. \quad (33)$$

*Proof.* Under the conditions that  $\|\sigma\tilde{\mathbf{L}}\|_F \ll \|\mathbf{L}\|_F$  and  $\lambda_k$  has multiplicity 1, it is shown in [17, Ch. II, Eqs. (2.21) and (2.33)]

$$\tilde{\lambda}_k = \text{tr}(\tilde{\mathbf{L}} \mathbf{P}_k) \quad (34)$$

and  $\mathbf{P}_k$  is given based on a contour integral [17, Ch. I, Eq. (5.22)] and further simplified in [28] to (30). Substituting (30) in (34) and using  $\text{tr}(\tilde{\mathbf{L}} \boldsymbol{\psi}_k \boldsymbol{\Phi}_k^H) = \text{tr}(\boldsymbol{\Phi}_k^H \tilde{\mathbf{L}} \boldsymbol{\psi}_k)$  results in (32). The proof of (33) is also given in [17, Ch. II, Eq. (4.23)].  $\square$

**Remark.** We assumed that all  $\lambda_k$  have multiplicity 1, which is generally assumed when considering NFT for communication. Eigenvalues with higher multiplicities are possible [29] and could be used for communication [30]. Noise would make these eigenvalues split [17], complicating the analysis.

To compute the perturbation  $\tilde{b}_k$ , we apply a Taylor expansion around  $\sigma = 0$  to the perturbed version of (17):

$$\begin{aligned}\hat{b}_k &= \frac{\mathbf{u}_{k,2}^T \boldsymbol{\psi}_{k,2} + \sigma \mathbf{u}_{k,2}^T \tilde{\boldsymbol{\psi}}_{k,2} + \mathcal{O}(\sigma^2)}{\mathbf{u}_{k,1}^T \boldsymbol{\psi}_{k,1} + \sigma \mathbf{u}_{k,1}^T \tilde{\boldsymbol{\psi}}_{k,1} + \mathcal{O}(\sigma^2)} \\ &= \frac{\mathbf{u}_{k,2}^T \boldsymbol{\psi}_{k,2}}{\mathbf{u}_{k,1}^T \boldsymbol{\psi}_{k,1}} \left( 1 + \sigma \frac{\mathbf{u}_{k,2}^T \tilde{\boldsymbol{\psi}}_{k,2}}{\mathbf{u}_{k,2}^T \boldsymbol{\psi}_{k,2}} - \sigma \frac{\mathbf{u}_{k,1}^T \tilde{\boldsymbol{\psi}}_{k,1}}{\mathbf{u}_{k,1}^T \boldsymbol{\psi}_{k,1}} \right) + \mathcal{O}(\sigma^2).\end{aligned}\quad (35)$$

Using (27),  $\tilde{b}_k$  is given in terms of  $b_k$  and  $\mathbf{u}_{k,1}^T \boldsymbol{\psi}_{k,1}$  as

$$\tilde{b}_k = \frac{1}{\mathbf{u}_{k,1}^T \boldsymbol{\psi}_{k,1}} \left( \mathbf{u}_{k,2}^T \tilde{\boldsymbol{\psi}}_{k,2} - b_k \mathbf{u}_{k,1}^T \tilde{\boldsymbol{\psi}}_{k,1} \right) \quad (36)$$

or equivalently,

$$\tilde{b}_k = \frac{1}{\mathbf{u}_{k,1}^T \boldsymbol{\psi}_{k,1}} (b_k \mathbf{u}_{k,1}^T - \mathbf{u}_{k,2}^T) \mathbf{S}_k \tilde{\mathbf{L}} \boldsymbol{\psi}_k. \quad (37)$$

Both  $\tilde{\lambda}_k$  and  $\tilde{b}_k$  depend on  $\tilde{\mathbf{L}} \boldsymbol{\psi}_k$ . From (24) we can write

$$\tilde{\mathbf{L}} \boldsymbol{\psi}_k = \begin{pmatrix} \tilde{\mathbf{\Gamma}} \boldsymbol{\psi}_{k,2} \\ -\tilde{\mathbf{\Gamma}}^H \boldsymbol{\psi}_{k,1} \end{pmatrix}. \quad (38)$$

The first vector  $\tilde{\mathbf{\Gamma}} \boldsymbol{\psi}_{k,2}$  is the convolution of  $-j\tilde{c}[n]$  and  $\boldsymbol{\psi}_{k,2}[n]$ . From the commutative property of convolution, i.e.  $-j\tilde{c}[n] * \boldsymbol{\psi}_{k,2}[n] = -j\boldsymbol{\psi}_{k,2}[n] * \tilde{c}[n]$ , it can be reordered as

$$\tilde{\mathbf{\Gamma}} \boldsymbol{\psi}_{k,2} = -j \mathbf{J}_{k,2} \tilde{\mathbf{c}} \quad (39)$$

where  $\mathbf{J}_{k,2} \in \mathbb{C}^{M \times M}$  is a Toeplitz matrix whose first column is  $(\boldsymbol{\psi}_{k,2}[0] \dots \boldsymbol{\psi}_{k,2}[N] \ 0 \dots 0)^T$  and whose first row is  $(\boldsymbol{\psi}_{k,2}[0] \dots \boldsymbol{\psi}_{k,2}[-N] \ 0 \dots 0)$ . Similarly,

$$-\tilde{\mathbf{\Gamma}}^H \boldsymbol{\psi}_{k,1} = -j \mathbf{J}_{k,1} \boldsymbol{\Pi} \tilde{\mathbf{c}}^* \quad (40)$$

where  $\mathbf{J}_{k,1}$  is defined similarly to  $\mathbf{J}_{k,2}$ , and  $\boldsymbol{\Pi}$  is an order-reversing matrix, i.e., an anti-diagonal matrix with the anti-diagonal elements equal to one. Equation (38) becomes

$$\tilde{\mathbf{L}} \boldsymbol{\psi}_k = -j \begin{pmatrix} \mathbf{J}_{k,2} \tilde{\mathbf{c}} \\ \mathbf{J}_{k,1} \boldsymbol{\Pi} \tilde{\mathbf{c}}^* \end{pmatrix} = \boldsymbol{\Sigma}_k \begin{pmatrix} \Re \tilde{\mathbf{c}} \\ \Im \tilde{\mathbf{c}} \end{pmatrix} \quad (41)$$

with

$$\boldsymbol{\Sigma}_k = \begin{pmatrix} -j \mathbf{J}_{k,2} & \mathbf{J}_{k,2} \\ -j \mathbf{J}_{k,1} \boldsymbol{\Pi} & -\mathbf{J}_{k,1} \boldsymbol{\Pi} \end{pmatrix}. \quad (42)$$

### B. Statistics of $\tilde{\lambda}_k$

Consider the perturbation term  $\tilde{\lambda}_k$  in (32). Using (41),

$$\tilde{\lambda}_k = \frac{1}{\boldsymbol{\phi}_k^H \boldsymbol{\psi}_k} \boldsymbol{\phi}_k^H \boldsymbol{\Sigma}_k \begin{pmatrix} \Re \tilde{\mathbf{c}} \\ \Im \tilde{\mathbf{c}} \end{pmatrix} = \mathbf{d}_k \begin{pmatrix} \Re \tilde{\mathbf{c}} \\ \Im \tilde{\mathbf{c}} \end{pmatrix} \quad (43)$$

where  $\mathbf{d}_k$  is a horizontal vector defined as

$$\mathbf{d}_k = \frac{1}{\boldsymbol{\phi}_k^H \boldsymbol{\psi}_k} \boldsymbol{\phi}_k^H \boldsymbol{\Sigma}_k = \frac{1}{\boldsymbol{\psi}_k^T \boldsymbol{\Pi} \boldsymbol{\psi}_k} \boldsymbol{\psi}_k^T \boldsymbol{\Pi} \boldsymbol{\Sigma}_k. \quad (44)$$

The second equality uses  $\boldsymbol{\phi}_k^H = \boldsymbol{\psi}_k^T \boldsymbol{\Pi}$  (see (29)). Let  $\tilde{\boldsymbol{\lambda}} = (\tilde{\lambda}_1, \dots, \tilde{\lambda}_K)^T$ , and let  $\mathbf{D}$  be a matrix whose rows are the  $\mathbf{d}_k$ .

Then we have  $\tilde{\boldsymbol{\lambda}} = \mathbf{D} \begin{pmatrix} \Re \tilde{\mathbf{c}} \\ \Im \tilde{\mathbf{c}} \end{pmatrix}$ , or

$$\begin{pmatrix} \Re \tilde{\boldsymbol{\lambda}} \\ \Im \tilde{\boldsymbol{\lambda}} \end{pmatrix} = \begin{pmatrix} \Re \mathbf{D} \\ \Im \mathbf{D} \end{pmatrix} \begin{pmatrix} \Re \tilde{\mathbf{c}} \\ \Im \tilde{\mathbf{c}} \end{pmatrix}. \quad (45)$$

The matrix  $\mathbf{D}$  contains the normalized autocorrelation functions of the FC eigenvectors  $\boldsymbol{\psi}_k$  (see [15] for an alternative formulation). In time domain, these autocorrelation functions become the squared Jost solutions, which is in accordance with Eq. (47) of [14]. The dependence of the perturbation of the eigenvalues on the squared Jost solutions is well known [31].

From (45), since  $(\Re \tilde{\mathbf{c}}^T, \Im \tilde{\mathbf{c}}^T)^T$  has a jointly Gaussian distribution,  $(\Re \tilde{\boldsymbol{\lambda}}^T, \Im \tilde{\boldsymbol{\lambda}}^T)^T$  has a jointly Gaussian distribution with zero mean and covariance matrix,

$$\mathbf{C}_{\tilde{\boldsymbol{\lambda}}} = \begin{pmatrix} \Re \mathbf{D} \\ \Im \mathbf{D} \end{pmatrix} \mathbf{R}_{\tilde{\mathbf{c}}} (\Re \mathbf{D}^T, \Im \mathbf{D}^T). \quad (46)$$

### C. Statistics of $\tilde{b}_k$ coefficients

Like  $\tilde{\lambda}_k$ ,  $\tilde{b}_k$  is a linear combination of  $\Re \tilde{c}[n]$  and  $\Im \tilde{c}[n]$ . To see this more clearly, define

$$\mathbf{h}_k = \frac{1}{\mathbf{u}_{k,1}^T \boldsymbol{\psi}_{k,1}} (b_k \mathbf{u}_{k,1}^T - \mathbf{u}_{k,2}^T) \mathbf{S}_k \boldsymbol{\Sigma}_k.$$

Using (37), we have simply,

$$\tilde{b}_k = \mathbf{h}_k \begin{pmatrix} \Re \tilde{\mathbf{c}} \\ \Im \tilde{\mathbf{c}} \end{pmatrix}. \quad (47)$$

Let  $\tilde{\mathbf{b}} = (\tilde{b}_1, \dots, \tilde{b}_K)^T$ , and let  $\mathbf{H}$  be a matrix whose rows are the  $\mathbf{h}_k$ . Then we have  $\tilde{\mathbf{b}} = \mathbf{H} \begin{pmatrix} \Re \tilde{\mathbf{c}} \\ \Im \tilde{\mathbf{c}} \end{pmatrix}$ , or

$$\begin{pmatrix} \Re \tilde{\mathbf{b}} \\ \Im \tilde{\mathbf{b}} \end{pmatrix} = \begin{pmatrix} \Re \mathbf{H} \\ \Im \mathbf{H} \end{pmatrix} \begin{pmatrix} \Re \tilde{\mathbf{c}} \\ \Im \tilde{\mathbf{c}} \end{pmatrix}. \quad (48)$$

Thus,  $(\Re \tilde{\mathbf{b}}^T, \Im \tilde{\mathbf{b}}^T)^T$  has a jointly Gaussian distribution with zero mean and covariance matrix,

$$\mathbf{C}_{\tilde{\mathbf{b}}} = \begin{pmatrix} \Re \mathbf{H} \\ \Im \mathbf{H} \end{pmatrix} \mathbf{R}_{\tilde{\mathbf{c}}} (\Re \mathbf{H}^T, \Im \mathbf{H}^T). \quad (49)$$

### D. Cross-statistics of $\tilde{\lambda}_k$ and $\tilde{b}_k$

From (45) and (48), we obtain the cross-covariance matrix  $\mathbf{C}_{\tilde{\boldsymbol{\lambda}} \tilde{\mathbf{b}}} \triangleq \mathbb{E}[(\Re \tilde{\boldsymbol{\lambda}}^T, \Im \tilde{\boldsymbol{\lambda}}^T)^T (\Re \tilde{\mathbf{b}}^T, \Im \tilde{\mathbf{b}}^T)^T]$ :

$$\mathbf{C}_{\tilde{\boldsymbol{\lambda}} \tilde{\mathbf{b}}} = \begin{pmatrix} \Re \mathbf{D} \\ \Im \mathbf{D} \end{pmatrix} \mathbf{R}_{\tilde{\mathbf{c}}} (\Re \mathbf{H}^T, \Im \mathbf{H}^T). \quad (50)$$

**Corollary.** *Up to the first-order approximation in  $\sigma$ , the eigenvalues  $\tilde{\lambda}_k$  of the noisy signal have a joint Gaussian distribution with means  $\lambda_k$  and covariance matrix  $\sigma^2 \mathbf{C}_{\tilde{\boldsymbol{\lambda}}}$ . The spectral coefficients  $\tilde{b}_k$  have a joint Gaussian distribution with means  $b_k$  covariance matrix  $\sigma^2 \mathbf{C}_{\tilde{\mathbf{b}}}$ . The cross-covariances between the  $\tilde{\lambda}_k$  and the  $\tilde{b}_k$  are  $\sigma^2 \mathbf{C}_{\tilde{\boldsymbol{\lambda}} \tilde{\mathbf{b}}}$ .*

## V. NUMERICAL VALIDATION

### A. Accuracy of FC in the noiseless case

We measured the accuracy of the computation of  $\{\lambda_k, b_k\}$  using (10) and (17) for three different pulses:

- a 2-soliton with  $\lambda_k = [0.6j, 0.3j]$  and  $b_k = [\frac{1}{3}j, \frac{1}{3}j]$
- a 5-soliton with  $\lambda_k = [1.5j, 1.2j, 0.9j, 0.6j, 0.3j]$  and, respectively,  $b_k = [0.8855 + 0.1109j, -1.4293 - 0.6778j, 1.0701 + 0.2486j, -0.0965 + 1.0385j, 0.3345 + 0.8551j]$

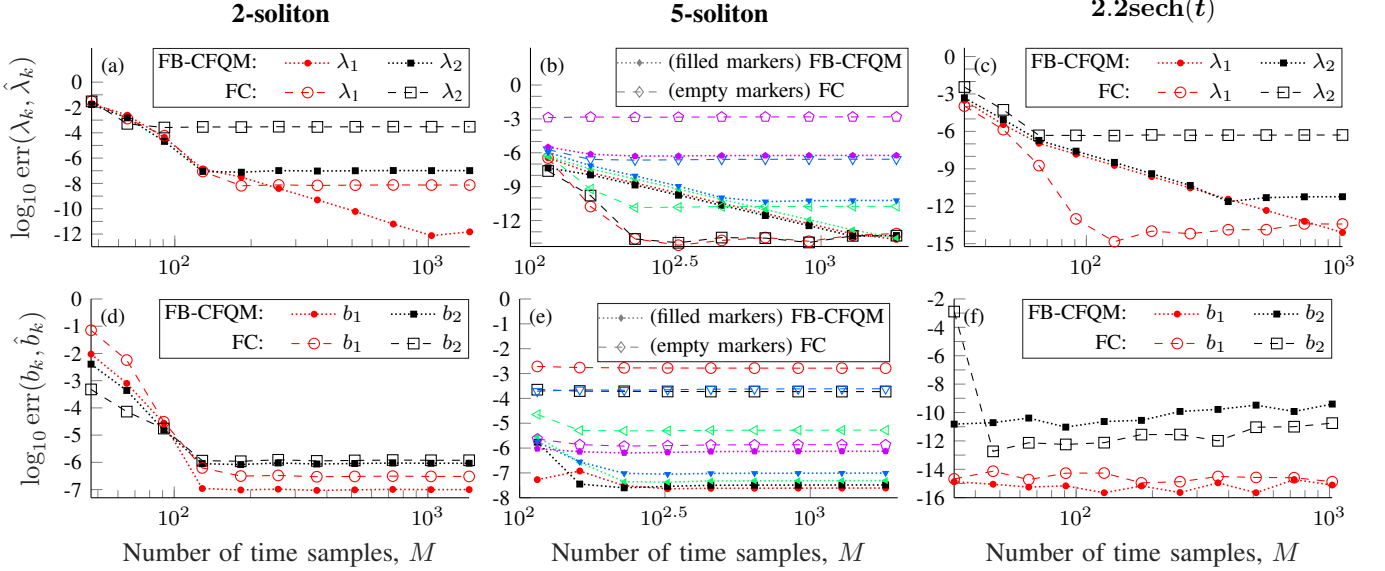


Fig. 2. Error in the computation of the discrete spectrum of different pulses. First column: error in  $\lambda_k$  (a) and  $b_k$  (d) for a 2-soliton. Second column: errors for a 5-soliton, with legend:  $\bullet$  ( $\lambda_1, b_1$ ),  $\blacksquare$  ( $\lambda_2, b_2$ ),  $\blacktriangleleft$  ( $\lambda_3, b_3$ ),  $\blacktriangledown$  ( $\lambda_4, b_4$ ),  $\blacklozenge$  ( $\lambda_5, b_5$ ). Third column: errors for  $q(t) = 2.2\text{sech}(t)$ .

- the pulse

$$q(t) = 2.2\text{sech}(t) \quad (51)$$

which has known nonzero continuous and discrete spectra [32]. The discrete spectrum is  $\lambda_k = [1.7, 0.7]$  and  $b_k = [-1, 1]$ .

We used the Darboux algorithm with double precision floating-point accuracy to generate the solitons, and then computed the discrete spectrum of the pulses using FB-CFQM and FC. For our FC method, we used tail truncation and Hann windows  $w_1[n]$  and  $w_2[n]$  (see (17)). We used a time interval with fixed length  $T$ , and varied the number of time samples by varying the sampling period. We used  $T = 35.3$  for the 2-soliton and the 5-soliton, and  $T = 24.0$  for the sech pulse. We compared the results of FB-CFQM and FC in terms of error:

$$\text{err}(\lambda_k, \hat{\lambda}_k) \triangleq \left( |\hat{\lambda}_k - \lambda_k| \right) / |\lambda_k| \quad (52)$$

where  $\hat{\lambda}_k$  is the eigenvalue obtained using FB-CFQM or FC, and  $\lambda_k$  is the original eigenvalue.  $\text{err}(b_k, \hat{b}_k)$  is defined similarly. The results in Fig. 2 show that Our FC method provides rather precise estimates of  $b_k$  (especially for 2-soliton and sech pulse, resp. Fig. 2 (d) and (f)). However, FB-CFQM has overall more precise estimates, especially when the number of samples is large.

### B. Accuracy of the FC perturbation analysis in the noisy case

To validate our proposed closed-form expressions for the covariance matrix of the eigenvalues (46) and spectral coefficients (49), we simulated the same three pulses of the previous section, using  $M = 365$  samples for the 2-soliton,  $M = 909$  for the 5-soliton, and  $M = 329$  for the sech pulse. Using higher values of  $M$  did not have any significant effect on the

resulting covariances. We then added AWGN  $\sigma\tilde{q}[m]$  to the three pulses. We define the signal-to-noise ratio (SNR) as:

$$\text{SNR} = \frac{1}{M\sigma^2} \sum_{m=-N}^N |q[m]|^2. \quad (53)$$

For each value of SNR, we generated 1024 realizations of noisy noise and computed the discrete spectrum of the noisy pulse using the FC and FB-CFQM. From this data, we estimated the covariance matrix of  $\lambda_k$  and of  $b_k$  for the FC and FB-CFQM case, and compared it with our analytic covariance matrices given by (46) and (49). For clarity of presentation, we only plot the following entries

$$\sigma_{\lambda_k}^2 \triangleq \sigma^2 \text{E} \left[ (\Re \tilde{\lambda}_k)^2 \right] + \sigma^2 \text{E} \left[ (\Im \tilde{\lambda}_k)^2 \right] \quad (54)$$

$$|\Re \sigma_{\lambda_1 \lambda_2}| \triangleq \sigma^2 \left| \text{E} \left[ \Re \tilde{\lambda}_1 \Re \tilde{\lambda}_2 + \Im \tilde{\lambda}_1 \Im \tilde{\lambda}_2 \right] \right| \quad (55)$$

Similar quantities are defined and plotted for  $b_k$ . We also compare the variances  $\sigma_{\lambda_k}^2$  of our method with the ones obtained from the time-domain method in [2]. Both methods obtain fairly the same  $\sigma_{\lambda_k}^2$  as shown in Fig. 3. For the 2-soliton, we set the SNR to 10 dB and used  $b_k = [\frac{1}{3}j, \frac{1}{3}j \exp(j\alpha)]$ . In the first column of Fig. 3, we plot  $\sigma_{\lambda_k}^2$  and  $|\Re \sigma_{\lambda_1 \lambda_2}|$  as a function of the phase difference  $\alpha$  between the spectral coefficients. As we already reported in [15], we see that the eigenvalues of 2-solitons where  $b_1$  and  $b_2$  have equal phase (or equivalently,  $Q_d(\lambda_1)$  and  $Q_d(\lambda_2)$  have *opposite* phase) are less robust to noise.

In the second and third columns of Fig. 3, we vary the SNR and plot  $\sigma_{\lambda_k}^2$  for the 5-soliton, and both  $\sigma_{\lambda_k}^2$  and  $|\Re \sigma_{\lambda_1 \lambda_2}|$  for the sech pulse. Our analytic expressions for the covariances (solid lines) very accurately predict the numerical covariances obtained using FC and FB-CFQM. For very low SNR, the computation of the Jost solutions using FC becomes numerically unstable, and the ringing in Fig. 1 increases considerably.

This makes the estimation of  $b_1$  with FC challenging, especially for the sech pulse. The analytic covariance matrix is computed from the noiseless pulse and is thus not affected by this. Our analytic covariances are in all cases very close to the lowest numerical ones (either FB-CFQM or FC).

Fig. 4 shows the full covariance matrix obtained with FC

$$\sigma^2 \mathbf{C} \triangleq \sigma^2 \begin{pmatrix} \mathbf{C}_{\lambda}^{\bar{\lambda}} & \mathbf{C}_{\lambda \bar{b}}^{\bar{\lambda}} \\ \mathbf{C}_{\lambda \bar{b}}^{\bar{\lambda}} & \mathbf{C}_{\bar{b}}^{\bar{b}} \end{pmatrix} \quad (56)$$

for the 2-soliton with SNR=10 dB and  $\alpha = \pi$  (i.e.,  $b_k = [\frac{1}{3}j, -\frac{1}{3}j]$ ). The covariance matrices obtained with FB-CFQM and with our analytic formulas (46), (49), (50) were very close to the FC result. Namely, the errors between them were

$$\|\mathbf{C}^{(\text{FC})} - \mathbf{C}^{(\text{analytic})}\|_{\text{F}}^2 / \|\mathbf{C}^{(\text{FC})}\|_{\text{F}}^2 \approx 0.0035 \quad (57a)$$

$$\|\mathbf{C}^{(\text{FC})} - \mathbf{C}^{(\text{FB-CFQM})}\|_{\text{F}}^2 / \|\mathbf{C}^{(\text{FC})}\|_{\text{F}}^2 \approx 0.0039 \quad (57b)$$

$$\|\mathbf{C}^{(\text{FB-CFQM})} - \mathbf{C}^{(\text{analytic})}\|_{\text{F}}^2 / \|\mathbf{C}^{(\text{analytic})}\|_{\text{F}}^2 \approx 0.0032. \quad (57c)$$

We observe in Fig. 4 that all real parts ( $\Re\lambda_k, \Re b_k$ ) are correlated with each other, and so are the imaginary parts ( $\Im\lambda_k, \Im b_k$ ), but there is little correlation between any real part and any imaginary part. Similarly to 1-solitons, the covariances of the  $\Re\lambda_k$  are smaller than those of the  $\Im\lambda_k$ .

## VI. CONCLUSION

We extended the Fourier Collocation (FC) method [16, Section 2.4.3] to compute the full discrete spectrum ( $\lambda_k$  and  $b(\lambda_k)$ ) of an arbitrary pulse. We showed numerically that our extended FC method estimates the discrete spectrum rather precisely with small number of samples. In comparison to the state-of-the-art FB-CFQM algorithm, both algorithms have a comparable estimation error for small number of samples. However, the FB-CFQM estimation errors decrease monotonically in number of samples while the FC estimation errors saturates to an error floor at some number of samples.

We applied perturbation theory of linear operators [17] to our method and derived analytic expressions for the second-order statistics of the discrete spectrum (eigenvalues and spectral amplitudes) of a pulse contaminated with additive white Gaussian noise. Our simulations show that our expressions very accurately predict the numerical statistics. Our expressions, though involved, are much faster than Monte-Carlo simulations and could be used to design better NFT transmission systems by avoiding combinations of spectral parameters that are less robust to noise.

This work assumes an AWGN channel. In optical fiber, usually a distributed noise model is assumed, where AWGN noise is added incrementally along the fiber. Our work can be extended to the distributed model by integrating our ( $z$ -dependent) analytic covariances along the  $z$  variable, similarly to [14]. This is left for future work.

## VII. ACKNOWLEDGMENT

The authors would like to thank Shrinivas Chimmalgi for pointing out numerical mistakes in evaluation of the FB-CFQM algorithm in the earlier version.

## REFERENCES

- [1] M. Ablowitz and H. Segur, *Solitons and the Inverse Scattering Transform*. Society for Industrial and Applied Mathematics, 1981.
- [2] M. I. Yousefi and F. R. Kschischang, "Information Transmission Using the Nonlinear Fourier Transform, Parts I-III," *IEEE Trans. Inf. Theory*, vol. 60, no. 7, pp. 4312–4369, July 2014.
- [3] R. J. Essiambre, G. Kramer, P. J. Winzer, G. J. Foschini, and B. Goebel, "Capacity Limits of Optical Fiber Networks," *J. Lightw. Technol.*, vol. 28, no. 4, pp. 662–701, Feb 2010.
- [4] S. K. Turitsyn *et al.*, "Nonlinear Fourier transform for optical data processing and transmission: advances and perspectives," *Optica*, vol. 4, no. 3, pp. 307–322, Mar 2017.
- [5] V. Aref, S. T. Le, and H. Buelow, "Modulation Over Nonlinear Fourier Spectrum: Continuous and Discrete Spectrum," *J. Lightw. Technol.*, vol. 36, no. 6, pp. 1289–1295, March 2018.
- [6] S. Hari, M. I. Yousefi, and F. R. Kschischang, "Multi-eigenvalue Communication," *J. Lightw. Technol.*, vol. 34, no. 13, pp. 3110–3117, July 2016.
- [7] S. Civelli, S. K. Turitsyn, M. Secondini, and J. E. Prilepsky, "Polarization-multiplexed nonlinear inverse synthesis with standard and reduced-complexity NFT processing," *Opt. Express*, vol. 26, no. 13, pp. 17360–17377, Jun 2018.
- [8] T. Gui, T. H. Chan, C. Lu, A. P. T. Lau, and P.-K. A. Wai, "Alternative decoding methods for optical communications based on nonlinear fourier transform," *J. Lightw. Technol.*, vol. 35, no. 9, pp. 1542–1550, May 2017.
- [9] S. T. Le, K. Schuh, F. Buchali, and H. Buelow, "100 Gbps b-modulated Nonlinear Frequency Division Multiplexed Transmission," in *Optical Fiber Commun. Conf. (OFC)*. Optical Society of America, 2018.
- [10] S. Wahls, "Second Order Statistics of the Scattering Vector Defining the D-T Nonlinear Fourier Transform," in *SCC 2017; 11th Int. ITG Conf. Systems, Commun. and Coding*, Feb 2017.
- [11] J. P. Gordon and H. A. Haus, "Random walk of coherently amplified solitons in optical fiber transmission," *Opt. Lett.*, vol. 11, no. 10, pp. 665–667, Oct 1986.
- [12] Q. Zhang and T. H. Chan, "A Gaussian noise model of spectral amplitudes in soliton communication systems," in *2015 IEEE 16th Int. Workshop on Signal Process. Advances in Wireless Commun. (SPAWC)*, June 2015, pp. 455–459.
- [13] S. A. Derevyanko, S. K. Turitsyn, and D. A. Yakushev, "Non-Gaussian statistics of an optical soliton in the presence of amplified spontaneous emission," *Opt. Lett.*, vol. 28, no. 21, pp. 2097–2099, Nov 2003.
- [14] L. Prati and L. Barletti, "Some results on discrete eigenvalues for the Stochastic Nonlinear Schrödinger Equation in fiber optics," *Commun. in Applied and Industrial Mathematics*, vol. 9, no. 1, pp. 87 – 103, 2018.
- [15] J. Garcia and V. Aref, "Statistics of the Eigenvalues of a Noisy Multi-Soliton Pulse," in *European Conf. Optical Commun. (ECOC)*, Sept 2018.
- [16] J. Yang, *Nonlinear Waves in Integrable and Nonintegrable Systems*. Society for Industrial and Applied Mathematics, 2010.
- [17] T. Kato, *Perturbation Theory for Linear Operators*. Springer, 1995.
- [18] G. P. Agrawal, *Nonlinear Fiber Optics*, 4th ed. Academic Press, 2012.
- [19] S. Wahls, "Generation of Time-Limited Signals in the Nonlinear Fourier Domain via b-Modulation," in *2017 European Conf. Optical Commun. (ECOC)*, Sept 2017.
- [20] L. Faddeev, A. Reyman, and L. Takhtajan, *Hamiltonian Methods in the Theory of Solitons*. Springer Berlin Heidelberg, 2007.
- [21] S. Hari and F. R. Kschischang, "Bi-Directional Algorithm for Computing Discrete Spectral Amplitudes in the NFT," *J. Lightw. Technol.*, vol. 34, no. 15, pp. 3529–3537, Aug 2016.
- [22] V. Aref, "Control and Detection of Discrete Spectral Amplitudes in Nonlinear Fourier Spectrum," *ArXiv e-prints*, May 2016.
- [23] S. Chimmalgi, P. J. Prins, and S. Wahls, "Fast Nonlinear Fourier Transform Algorithms Using Higher Order Exponential Integrators," *arXiv e-prints*, Dec. 2018.
- [24] V. Matveev and M. Salle, *Darboux Transformations and Solitons*, ser. Springer series in nonlinear dynamics. Springer-Verlag, 1991.
- [25] R. B. Blackman and J. W. Tukey, "The measurement of power spectra from the point of view of communications engineering Part I," *The Bell System Technical Journal*, vol. 37, no. 1, pp. 185–282, Jan 1958.
- [26] A. Span, V. Aref, H. Blow, and S. T. Brink, "On time-bandwidth product of multi-soliton pulses," in *IEEE Int. Symp. Inf. Theory (ISIT)*, June 2017, pp. 61–65.
- [27] U. G. Rothblum, "Resolvent expansions of matrices and applications," *Linear Algebra and its Applications*, vol. 38, pp. 33 – 49, 1981.
- [28] G. Rothblum, "Computation of the eigenprojection of a nonnegative matrix at its spectral radius". Berlin, Heidelberg: Springer Berlin Heidelberg, 1976, pp. 188–201.

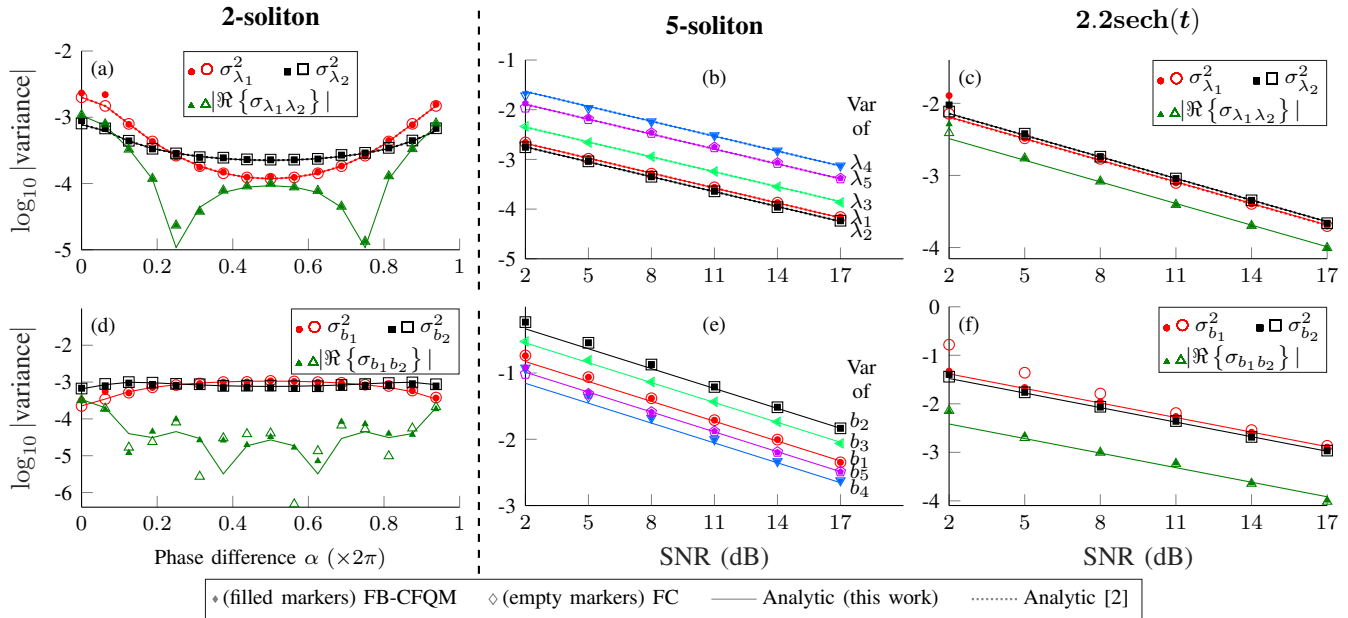


Fig. 3. Statistics of the discrete spectrum of different noisy pulses. The first column gives the analytic and numerical second-order moments of  $\lambda_k$  (a) and  $b_k$  (d) of a noisy 2-soliton with SNR=10 dB, as a function of the phase difference  $\alpha$  between the  $b_1$  and  $b_2$ . The second column gives the moments of  $\lambda_k$  (b) and  $b_k$  (e) of a 5-soliton as a function of SNR. The third column (c) and (f) gives the moments for  $q(t) = 2.2\text{sech}(t)$  as a function of SNR.

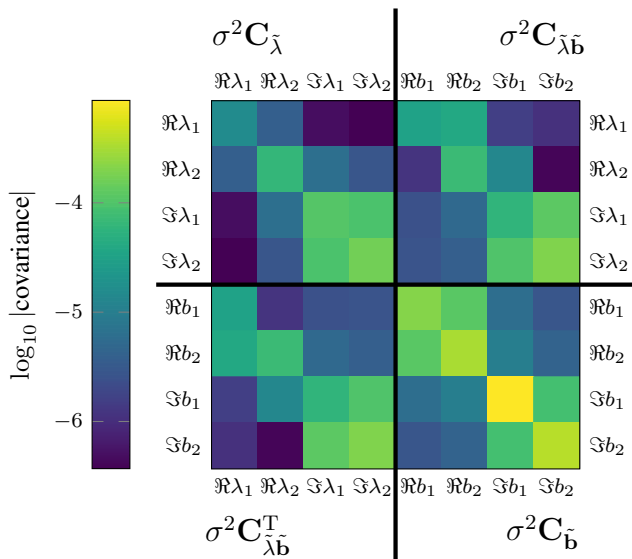


Fig. 4. Covariance matrix of  $\lambda_k$  and  $b_k$  for a 2-soliton with  $\lambda_k = [0.6j, 0.3j]$  and  $b_k = [\frac{1}{3}j, -\frac{1}{3}j]$  (SNR=10 dB). Note that the color scale is logarithmic.

- [29] E. Olmedilla, "Multiple pole solutions of the non-linear Schrödinger equation," *Physica D: Nonlinear Phenomena*, vol. 25, no. 1, pp. 330 – 346, 1987.
- [30] F. J. García-Gómez, "Communication Using Eigenvalues of Higher Multiplicity of the Nonlinear Fourier Transform," *J. Lightw. Technol.*, vol. 36, no. 23, pp. 5442–5450, Dec 2018.
- [31] D. J. Kaup, "A perturbation expansion for the zakharov-shabat inverse scattering transform," *SIAM Journal on Applied Mathematics*, vol. 31, no. 1, pp. 121–133, 1976.
- [32] J. Satsuma and N. Yajima, "Initial Value Problems of One-Dimensional Self-Modulation of Nonlinear Waves in Dispersive Media," *Progress of Theoretical Physics Supplement*, vol. 55, pp. 284–306, 1974.